Space-adjustable dark magneto-optical trap for efficient production of heteronuclear molecules

Zhujun Zhang (张竹君), Zhonghua Ji (姬中华), Zhonghao Li (李中豪), Jinpeng Yuan (元晋鹏), Yanting Zhao (赵延霆)*, Liantuan Xiao (肖连团), and Suotang Jia (贾锁堂)

State Key Laboratory of Quantum Optics and Quantum Optics Devices, Institute of Laser Spectroscopy, Shanxi University, Taiyuan 030006, China

**Corresponding author: zhaoyt@sxu.edu.cn*

Received May 17, 2015; accepted August 28, 2015; posted online October 7, 2015

We present a simple, robust, space-adjustable dark magneto-optical trap (MOT) for the efficient production of heteronuclear molecules. Double-mixed beams made up of repumping beams and depumping beams propagate in nearly opposite directions in the dark MOT. This optical arrangement can easily adjust the spatial positions of two clouds by changing the power ratio of the two repumping beams, and ensure a good overlap, which is very necessary for the production of heteronuclear molecules. The imaging of cold atoms by camera and the collision-induced loss rate obtained by recording the loading curve of the cold atoms show that we obtain a perfect overlap of atom clouds. The number of RbCs molecules with the double-mixed beams is improved by 70%, which is higher than the one with the single-mixed beam.

OCIS codes: 020.3320, 020.7010, 300.6360, 300.6390.
doi: 10.3788/COL201513.110201.

In recent years, ultracold atoms have played a key role in advancing many research fields[1,2]. Ultracold molecules also have attracted the attention of many research groups around the world that study cold atoms[3–5]. In particular, the preparation of ultracold heteronuclear molecules is an important subject[6]. This is mainly because heteronuclear molecules have abundant rovibrational levels, tunable dipole–dipole interaction, and permanent electric dipole moment, and they are easier to be controlled with an electric field. Heteronuclear molecules have been widely used in many fields, such as ultracold chemistry[7,8], precision measurement[9], ultracold collisions[10], high resolution spectroscopy[11], quantum computing[12], and quantum storage[13].

Most groups use photoassociation (PA) technology to produce ultracold heteronuclear molecules because of its higher efficiency in molecular production compared to Feshbach technology[14] and its simple operation. It has been operated in alkali atoms, such as KRb[15], RbCs[16], LiCs[11], and rare-earth elements, such as YbRb[17]. During the process of PA, two different ground-state atoms absorb a photon and form a bound excited-state molecule. As the excited-state molecule is not stable, it will form a stable ground-state molecule after spontaneous radiation or stimulated radiation, or will return to separate atoms. Compared to the preparation of homonuclear molecules by PA, it is much more difficult to produce heteronuclear molecules due to the potential energy characteristics of the ground state and excited state. The free-bound Frank–Condon factor of PA for heteronuclear molecules is significantly smaller than that for homonuclear molecules. So the former process needs a larger atomic density and a lower collision-induced loss rate, which are two main influencing factors in the production process. Researchers always use a dark magneto-optical trap (MOT) to solve these problems. Ketterle *et al.*[18] confined about 10^{12} sodium atoms per cubic centimeter in a dark MOT, whose atomic density is much higher than that in a normal MOT. Our group also studied ultracold atoms and molecules in a dark MOT via depumping the cesium cold atoms into the dark hyperfine ground state, and found that the collision rate decreases by half and the density of the atom clouds increases by one order[19].

When dark MOT technology is used in the production of heteronuclear molecules, researchers exert a lot of effort on the overlap of two clouds, which is necessary for the efficient production of heteronuclear molecules. The difficulty of the overlap problem arises from the optical arrangement of trapping beams and mixed beams (depumping beam and repumping beam) for the two species of atoms. Two independent series of trapping beams are usually designed to easily adjust spatial positions; However, this initially induces bad overlapping for the two clouds in the MOT. When the mixed beam is added along one direction or perpendicular directions in a normal dark MOT, the scattering forces on the two species of atoms are unbalanced, which will induce the two species of atoms to separate much more. In addition, the low utilization efficiency of the repumping beam will lead to a lower number of initial atoms produced in MOT and in the dark state.

We propose here a method that can easily control the spatial positions of two special atoms by using double-mixed beams in near-counter propagation. The spatial positions of two clouds are adjusted to realize a complete overlap by changing the power ratio of two repumping beams. By calculating the overlap ratio, we defined and

measured the collision-induced loss rate of atoms, with which we can confirm whether the overlap of atoms is qualified. We will compare the intensity of produced $RbCs^+$ molecule ions in double-mixed beams with the intensity in a single-mixed beam.

The experiment is operated in a commercially available stainless-steel chamber. The vacuum background pressure in chamber is about 1.3×10^{-7} Pa. The quadrupole magnetic field is provided by a pair of anti-Helmholtz coils with a magnetic gradient of 15 G/cm in the center of the trap.

The Rb and Cs atoms are trapped in a dark MOT. Figure 1 is the simple schematic diagram of the energy levels that are used to obtain the atoms in the lowest hyperfine states in our experiment. The trapping laser and depumping laser for the Rb atoms are produced by the same diode laser. The case is similar for Cs atoms. The repumping lasers for Rb and Cs are produced by another two diode lasers. The detunings of the trapping laser for Rb and Cs with acousto-optic modulators are 12.5 MHz below the ^{85}Rb $5^2S_{1/2}(F=3) \rightarrow 5^2P_{3/2}(F'=4)$ resonance transition and 15 MHz below the 133Cs $6^2S_{1/2}(F=4) \rightarrow 6^2P_{3/2}(F'=5)$ resonance transition, respectively. The frequencies of the repumping lasers for Rb and Cs are the $5^2S_{1/2}(F=2) \rightarrow 5^2P_{3/2}(F'=3)$ resonance transition and the $6^2S_{1/2}(F=3) \rightarrow 6^2P_{3/2}(F'=4)$ resonance transition, respectively. The frequencies of the depumping lasers for Rb and Cs are stabilized to the $5^2S_{1/2}(F=3) \rightarrow 5^2P_{3/2}(F'=2)$ resonance transition and the $6^2S_{1/2}(F=4) \rightarrow 6^2P_{3/2}(F'=4)$ resonance transition, respectively. They are used to make the Rb and Cs atoms in the $5^2S_{1/2}(F=2)$ and $6^2S_{1/2}(F=3)$ hyperfine states in the dark MOT.

Figure 2 is a brief diagram of the optical elements in the near-vacuum chamber. The trapping beams and repumping beams of Rb and Cs are combined in order to use the same optical path and optical components. This arrangement not only saves space, but also makes the initial atom clouds in the MOT have a good overlap in the space location. The trapping beams of Rb and Cs are combined together by a dichroic mirror and then are divided into three pairs by polarizing beam splitters (PBSs) and half-wave plates. The powers of the trapping beams, both of which have diameters ~20 mm, for Rb and Cs are ~26 and ~35 mW, respectively. There are two repumping beams, both with powers of ~10 mW and diameters of ~20 mm. The two repumping beams are combined together by the PBS and half-wave plates. The powers of the depumping beams, both of which have diameters of ~3 mm, for the Rb and Cs atoms are 60 and 70 μW, respectively. We also combine the two depumping beams with the PBS and half-wave plates. Then, we put a black dot with a diameter of 3 mm at the center of the combined repumping beams to produce the dark region. The combined depumping beams fill the dark region of the combined repumping beams and make the cold atoms transfer to the lower hyperfine state in the dark MOT. At the same time, we use a PBS to divide the mixed beam into two beams before it enters the chamber. Then, the double-mixed beams both finally pass through a pair of lenses into the vacuum chamber. The power ratio of the two repumping beams, labeled as P1 and P2, as shown in Fig. 2, can be controlled by changing the degrees of the half-wave plate for each atom. Here, the total powers of the repumping beams for both atoms are constant. Thus, the scattering force acting on the atom clouds can be controlled, which leads to the movement of the two clouds. This method can ensure a good spatial overlap of the mixed atoms.

The numbers of Rb and Cs atoms we produced in the dark state is about 8×10^7 and 1×10^8, respectively. There are three CCD cameras, two of which are placed in the horizontal direction, and one of which is placed in the vertical direction to expediently verify the spatial overlap of the two clouds. The atomic fluorescence signal is collected by a Si-avalanche photodiode module (Licel APD–1.5).

The narrow linewidth (<60 kHz), tunable CW Ti:sapphire laser (M Squared, Sols Tis) acts as the PA

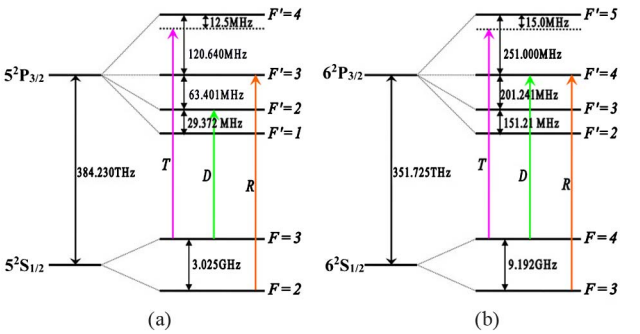

Fig. 1. Energy levels diagram of (a) ^{85}Rb and (b) ^{133}Cs in dark MOT. T: trapping laser, D: depumping laser, R: repumping laser.

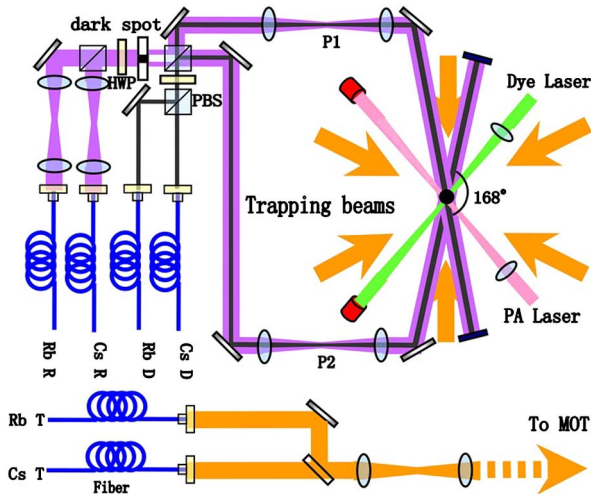

Fig. 2. Brief diagram of optical elements in near-vacuum chamber. The angle between the double-mixed beams of the repumping lasers and depumping lasers is 168°.

laser. The output power is about 800 mW. The Gaussian diameter of the PA beam is about 0.5 mm. The RbCs molecule is produced by PA in the dark MOT. The ionization laser is provided by a pulsed dye laser (Spectra-Physics, Sirah), which is pumped by a Nd:YAG frequency doubled laser (532 nm). The pulse duration of the ionization laser is 8 ns, and the repetition rate is 10 Hz. The dye laser energy used in the experiment is 1.5 mJ. The absolute frequency of the PA laser is measured by a wavelength meter (HighFinesse-Angstrom, WS/7R). The accuracy of the wavelength meter is 60 MHz. We use time-of-flight (TOF) mass spectrometry technology to detect the ionized atoms and molecules because they have the same electrical charges, but different masses.

To observe the overlap of the two clouds, we use the CCD to directly achieve the space location. By counting the pixel point of the CCD, we can calculate the overlap ratio of the two clouds, which is defined as

$$\eta = 1 - \frac{d}{R_{\mathrm{Rb}} + R_{\mathrm{Cs}}}, \tag{1}$$

where d is the center-to-center distance of the two clouds, and R_{Rb} and R_{Cs} are the radii of the Rb and Cs atom clouds, respectively.

Figure 3(a) shows the spatial positions of the Rb and Cs atom clouds with different power ratios of the two repumping beams of the double-mixed beams. The power ratios P1:P2 of the Rb repumping beams are set to be 0, 0.47, and 4.44 from left to right, and the overlap ratios are measured to be 0, 0.65, and 1 based on the definition of Eq. (1). The power ratios P1:P2 of the Cs repumping beams are measured to be 1.1, 0.1, and 0.067 for the three cases. The narrow-range variety of the power ratios of the Cs repumping beams result in less movement in the Cs atom cloud, compared with the Rb atom cloud.

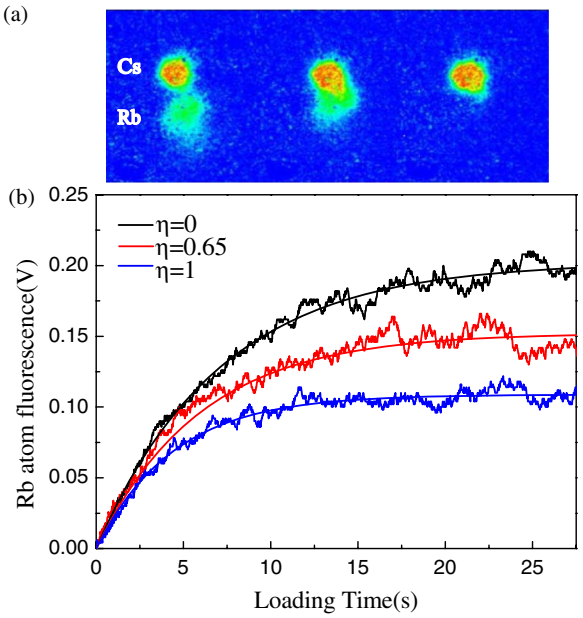

Fig. 3. (a) Spatial position of Rb and Cs atom clouds with different power ratios of two repumping beams in double-mixed beams. The power ratios P1:P2 of the Rb repumping beams are set to be 0, 0.47, and 4.44 from left to right, and the overlap ratios are measured to be 0, 0.65, and 1 based on the definition of Eq. (1). (b) The corresponding loading curves of the Rb atoms immerged in Cs atoms. The obtained collision-induced loss rates are 0.14(1), 0.17(3), and 0.23(3) s^{-1} according to the theoretical fit of Eq. (3).

During the loading processes of the Rb atoms and Cs atoms, the Cs atoms have a great influence on the Rb atoms because of the inelastic collision between ultracold atoms[20]. When the overlap is better, the collision is much stronger. The inelastic collision-induced loss rate between ultracold atoms cannot be directly detected, but it can usually be calculated by recording cold atomic fluorescence in the loading process or decay process. Here, we introduce the loading curves of Rb atoms to calculate the loss rate of collision, which can also reflect the overlap ratio of the two clouds.

The number of cold atoms N in the loading process in the MOT along with the change of time t can be expressed as[21]

$$\frac{\mathrm{d}N}{\mathrm{d}t} = L - \gamma_b N - \beta \int_r n^2(r,t)\mathrm{d}^3 r, \tag{2}$$

where L is loading rate of the cold atoms, γ_b is the collision loss rate between the ultracold atoms and background gas, β is collision rate of the ultracold atoms, and n is the density of the ultracold atoms.

Under the constant density approximation, the density of the cold atoms will be a fixed value and will not change any more even as the loading time increases. Then, the number of atoms increases with the increase of the atom cloud's volume[22]. Under such an approximation, we consider the initial conditions of the cold atoms loading ($t = 0$, $N = 0$), and the number of cold atoms at any time in the MOT is

$$N = N_s(1 - e^{-(\gamma_b - \beta n)t}), \tag{3}$$

where N_s is the number of steady-state atoms in the MOT.

To detect cold Rb atomic fluorescence in the dark MOT, we use a narrow-band interference filter to eliminate the influence of other light. Figure 3(b) records the corresponding loading curves of the Rb atoms immerged in cold Cs atoms for the three cases shown in Fig. 3(a). From Fig. 3(b), we can see that the fluorescence intensity in the steady state decreases with the increase in the overlapping area of the two clouds, while the time of the loading curve becomes shorter. According to Eq. (3), we can calculate that the loss rates of collision are 0.14(1), 0.17(3), and 0.23(3) s^{-1} under the corresponding overlap ratios. It needs to be declared that the collision rate in the dark MOT is smaller than the value in the normal MOT (0.56 s^{-1}).

To verify the efficiency of our method, we compare the signal intensities of the $RbCs^+$ molecular ion from the

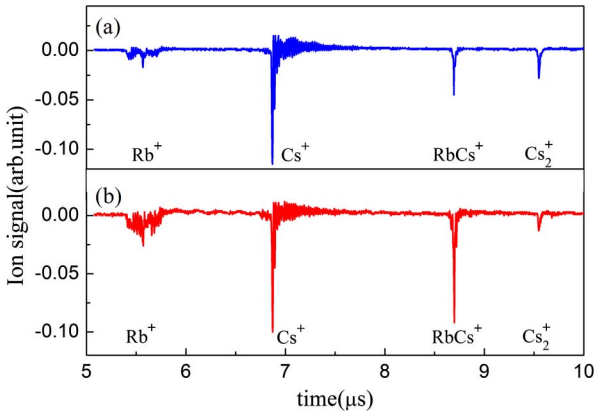

Fig. 4. Ion signal spectra of RbCs of (a) single-mixed beam and (b) double-mixed beams.

single-mixed beam and the double-mixed beams when the PA frequency is fixed at one rovibrational state of $(2)^3\Pi$ state (11724.083 cm^{-1})[23]. The other experimental parameters remain the same. The ion spectra are detected by TOF mass spectrometry and recorded by an oscilloscope, shown in Fig. 4. Comparing with the $RbCs^+$ molecular ion signal with the single-mixed beam, the signal clearly increases with the double-mixed beams. However, we do not observe any obvious enhancement for the atomic ion intensities of the Rb and Cs atoms. So this improvement benefits from the optimal overlap of the two clouds in the double-mixed beams.

We also measure the $RbCs^+$ molecular ion signals as a function of the PA laser intensity with the single-mixed beam and double-mixed beams. The range of the PA intensity increases up to 200 W/cm^2. As shown in Fig. 5, the dots are the $RbCs^+$ signals from the single-mixed beam, and the triangles are the $RbCs^+$ signals from the double-mixed beams. The two serial signals are fitted independently by the PA rate[24]

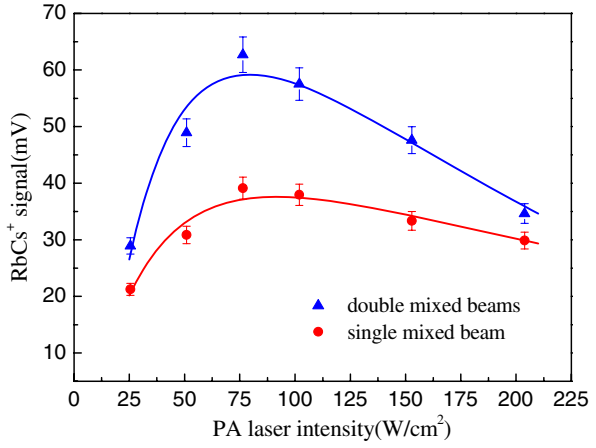

Fig. 5. $RbCs^+$ molecular ion intensities of single-mixed beam and double-mixed beams as functions of PA laser intensity. The solid lines are the fitted results of the experiment data by Eq. (4).

$$|S|^2 = \frac{I \cdot I_S}{\frac{1}{4}(I + I_S)^2}, \tag{4}$$

where I is the PA intensity, and I_S is the PA saturation intensity. From Fig. 5, we can see that under the same PA laser intensity, the $RbCs^+$ molecular ion signals from the double-mixed beams are larger than that from the single-mixed beam, and the largest signal from the double-mixed beams is enhanced by 70% more than that from the single beam. The two atom clouds usually overlap about 80% and the RbCs molecular production rate in the metastable ground state is estimated to be 2.5×10^4 s^{-1} when we use a single-mixed beam[23]. After employing the double-mixed beams, the overlap ratio reaches nearly 100%, and the production rate is estimated to be 4.4×10^4 s^{-1}. For both cases, the $RbCs^+$ ion signal decreases after the maximum value as the PA intensity increases due to the saturation effect[25]. What we found here is that the double-mixed beams not only produce more molecules, but also build an easier space-adjustable setup for the overlap of two clouds. This indicates that the double-mixed beams have a very good enhancement effect on the production of heteronuclear molecules, and the method of the double-mixed beams of repumping beams and depumping beams we proposed is very effective.

A space-adjustable dark MOT is adopted to produce RbCs molecules from cold Rb and Cs atoms in the lowest hyperfine state. The three-dimensional spatial positions of the two clouds are adjusted by changing the power ratio of the repumping beams in the mixed beams in near-counter propagation. Using this technique, we finally have a perfect space overlap of atom clouds by imaging the cold atoms and measuring the collision-induced loss rate with the loading curves of the cold Rb atoms. Serial measurements for the $RbCs^+$ ion intensity as a function of the PA laser intensity verify the efficiency of our method. The ultracold $RbCs^+$ ion intensity of the double-mixed beams is enhanced by 70% more than the one of the single-mixed beam under the same conditions. This powerful method is not only useful for the production of all other heteronuclear molecules, but is also useful to researchers interested in atomic interaction[26,27].

This work was supported by the National 973 Program of China (No. 2012CB921603), the National Natural Science Foundation of China (Nos. 61275209, 11304189, 61378015, and 11434007), the NSFC Project for Excellent Research Team (No. 61121064), and PCSIRT (No. IRT13076).

References

1. X. Wang, H. Cheng, L. Xiao, B. Zheng, Y. Meng, L. Liu, and Y. Wang, Chin. Opt. Lett. **10**, 080201 (2012).
2. J. Wan, H. Cheng, Y. Meng, L. Xiao, P. Liu, X. Wang, Y. Wang, and L. Liu, Chin. Opt. Lett. **13**, 020201 (2015).
3. G. Quéméner and P. S. Julienne, Chem. Rev. **112**, 4949 (2012).
4. L. D. Carr, D. DeMille, R. V. Krems, and J. Ye, New J. Phys. **11**, 055049 (2009).

5. C. Chin, R. Grimm, P. Julienne, and E. Tiesinga, Rev. Mod. Phys. **82**, 1225 (2010).
6. D. Shi, Y. Liu, J. Sun, Z. Zhu, and X. Yang, Chin. Opt. Lett. **3**, 683 (2005).
7. H. Jing, J. Cheng, and P. Meystre, Phys. Rev. Lett. **101**, 073603 (2008).
8. H. Jing, J. Cheng, and P. Meystre, Phys. Rev. A **79**, 023622 (2009).
9. J. J. Hudson, D. M. Kara, I. J. Smallmanl, B. E. Sauer, M. R. Tarbutt, and E. A. Hinds, Nature **473**, 493 (2011).
10. M. D. Swallows, M. Bishof, Y. Lin, S. Blatt, M. J. Martin, A. M. Rey, and J. Ye, Science **331**, 1043 (2011).
11. J. Deiglmayr, A. Grochola, M. Repp, K. Mörtlbauer, C. Glück, J. Lange, O. Dulieu, R. Wester, and M. Weidemüller, Phys. Rev. Lett. **101**, 133004 (2008).
12. D. DeMill, Phys. Rev. Lett. **88**, 067901 (2002).
13. H. Jing, Y. Deng, and W. Zhang, Phys. Rev. A **80**, 025601 (2009).
14. J. J. Zirbel, K.-K. Ni, S. Ospelkaus, T. L. Nicholson, M. L. Olsen, P. S. Julienne, C. E. Wieman, J. Ye, and D. S. Jin, Phys. Rev. A **78**, 013416 (2008).
15. M. W. Mancini, G. D. Telles, A. R. L. Caires, V. S. Bagnato, and L. G. Marcassa, Phys. Rev. Lett. **92**, 133203 (2004).
16. J. M. Sage, S. Sainis, T. Bergeman, and D. DeMille, Phys. Rev. Lett. **94**, 203001 (2005).
17. N. Nemitz, F. Baumer, F. Münchow, S. Tassy, and A. Görlitz, Phys. Rev. A **79**, 061403 (2009).
18. W. Ketterle, K. B. Davis, M. A. Joff'e, A. Martin, and D. E. Pritchard, Phys. Rev. Lett. **70**, 2253 (1993).
19. L. R. Wang, Z. H. Ji, J. P. Yuan, Y. Yang, Y. T. Zhao, J. Ma, L. T. Xiao, and S. T. Jia, Chin. Phys. B **21**, 113402 (2012).
20. Z. H. Ji, J. Z. Wu, H. S. Zhang, T. F. Meng, J. Ma, L. R. Wang, Y. T. Zhao, L. T. Xiao, and S. T. Jia, J. Phys. B **44**, 025202 (2011).
21. C. Monroe, W. Swann, H. Robinson, and C. Wieman, Phys. Rev. Lett. **65**, 1571 (1990).
22. L. Marcassa, V. Bagnato, Y. Wang, C. Tsao, J. Weiner, O. Dulieu, Y. B. Band, and P. S. Julienne, Phys. Rev. A **47**, R4563 (1993).
23. Z. H. Ji, H. S. Zhang, J. Z. Wu, J. P. Yuan, Y. G. Yang, Y. T. Zhao, J. Ma, L. R. Wang, L. T. Xiao, and S. T. Jia, Phys. Rev. A **85**, 013401 (2012).
24. J. L. Bohn and P. S. Julienne, Phys. Rev. A **60**, 414 (1999).
25. J. P. Yuan, Z. H. Ji, Y. T. Zhao, Y. Yang, Y. G. Yang, L. T. Xiao, and S. T. Jia, J. Phys. Soc. Jpn. **82**, 084301 (2013).
26. S. B. Papp, J. M. Pino, and C. E. Wieman, Phys. Rev. Lett. **101**, 040402 (2008).
27. H. Jing, X. Zhao, and L. F. Buchmann, Phys. Rev. A **86**, 065801 (2012).